

Article

Verification and Analysis of the Problem-Dependent Multigroup Macroscopic Cross-Sections for Shielding Calculations

Xu Zhao ¹, Shengchun Shi ^{2,*}, Wen Xu ¹, Jiaju Hu ², Jun Wu ¹ and Bin Zhang ¹

¹ School of Nuclear Science and Engineering, North China Electric Power University, Beijing 102206, China; 18183744911@163.com (W.X.)

² Nuclear and Radiation Safety Center, Beijing 100082, China

* Correspondence: shishengchun@chinansc.cn

Abstract: Multigroup constants are the foundation of neutron and photon transport problems, and the accuracy of multigroup cross-sections has a significant impact on shielding calculation. Challenges have arisen in generating accurate multigroup macroscopic cross-sections for some problems using the widely used cross-section processing code TRANSX 2.15. We developed the multigroup neutron-photon macroscopic cross-section processing module in the shielding transport code ARES. The module is capable of handling the neutron-photon coupled master libraries in MATXS format and providing the problem-dependent multigroup macroscopic cross-sections tailored to each specific shielding physics problem. The self-designed problems with a single nuclide, as well as the iron and OKTAVIAN experiments, are used to verify and analyze the accuracy of neutron and photon macroscopic cross-sections. Results indicate that the macroscopic cross-sections, neutron flux and neutron-photon leakage spectrum obtained by the MGMXS module are consistent with corresponding reference values. As for the JANUS Phase I fixed source shielding benchmark, the relative differences in the reaction rate between the calculation results and experimental data are within 20%. The module provides better problem-dependent multigroup macroscopic cross-sections for neutron and photon shielding calculations that satisfy the accuracy requirements of engineering applications.

Keywords: shielding calculation; nuclear data library; MATXS format; multigroup cross-section



Citation: Zhao, X.; Shi, S.; Xu, W.; Hu, J.; Wu, J.; Zhang, B. Verification and Analysis of the Problem-Dependent Multigroup Macroscopic Cross-Sections for Shielding Calculations. *Energies* **2023**, *16*, 3366. <https://doi.org/10.3390/en16083366>

Academic Editors: Dan Gabriel Cacuci, Shichang Liu, Jingang Liang and Zhaoyuan Liu

Received: 14 March 2023

Revised: 5 April 2023

Accepted: 6 April 2023

Published: 11 April 2023



Copyright: © 2023 by the authors. Licensee MDPI, Basel, Switzerland. This article is an open access article distributed under the terms and conditions of the Creative Commons Attribution (CC BY) license (<https://creativecommons.org/licenses/by/4.0/>).

1. Introduction

Shielding calculations play an important role in the design of nuclear reactor systems, safety evaluations of devices and radiation assessments of personnel [1]. The key to shielding simulations is to solve the Boltzmann transport equation and obtain the neutron and photon flux distribution over the phase space. The discrete ordinates (S_N) [2] method is a mainstream deterministic approach for particle transport problems, and the reliability of nuclear data is crucial for S_N transport calculations. Shielding calculations take into account neutrons and photons. Suitable neutron and photon cross-sections are necessary for accurate shielding calculations.

Although the evaluated nuclear data libraries contain comprehensive pointwise reaction cross-sections for neutrons and photons, S_N transport codes do not directly use this data from the evaluations due to its high computational cost. The American Nuclear Society established an approach for developing multigroup cross-sections for radiation protection and shielding analysis of nuclear power plants, and it was recommended as an industry standard. The methodology for generating multigroup cross-sections contains a two-stage process. The first step is to process the ENDF-6 format evaluation of nuclear data libraries into a multigroup master library. The second step is to process the master library according to the physical characteristics of the problem, then generate a multigroup cross-sections working library. The problem-dependent multigroup macroscopic cross-sections in the

working library can be used in S_N transport calculations. Accurate shielding calculations depend on high-precision, problem-dependent multigroup macroscopic cross-sections for shielding materials.

Nuclear data processing codes are used to process and develop the evaluated nuclear data to produce a multigroup master library in a specific format. The NJOY [3] and AMPX [4], as well as the NECP-Atlas [5], developed by Xi'an Jiaotong University, are internationally recognized nuclear data processing codes. In addition, the Institute of Physics and Power Engineering (IPPE) in Russia modified the NJOY to generate the BNAB format [6] library for fast reactor shielding design. These codes have been used to create numerous neutron-photon coupled libraries both domestically and internationally to accommodate the characteristics of various reactor types. For instance, the Los Alamos National Laboratory developed the VITAMIN-B6 [7] library for light-water-reactor analysis. The Russian ABBN-RF2010 [8] library was designed for fast reactor analysis. The MUSE1.0 [9] library was developed by the North China Electric Power University for supercritical water reactor design and the KASHIL-E70 [10] library was created by the Korea Atomic Energy Research Agency for shielding calculations.

The multigroup master library is pseudoproblem-independent and requires processing and development by cross-section processing code for S_N transport codes (such as the Doors [11] code system). At present, many multigroup cross-section processing codes have been developed. The SCALE 6.2.4 [12] code system developed by Oak Ridge National Laboratory includes the resonance self-shielding processing modules BONAMI, CENTRM, PMC and NITAWL. In the resonance self-shielding correction, the unresolved resonance regions and the resolved resonance regions are treated separately, and the problem-dependent multigroup cross-sections with high precision are generated by combining the pointwise and multigroup nuclear data libraries. However, SCALE can only process multigroup master libraries in AMPX format and requires more computer storage and runtime. The CONSYST [13] code developed by IPPE is to link the ABBN constants with neutronic transport calculation codes. Nguyen [14] used the Monte Carlo code MCS to generate the multigroup cross-sections for fast reactor core calculations using nodal diffusion codes. In addition, with the development of computers, a number of multi-group cross-section generation codes have been developed that can directly process evaluated nuclear data files. Both the MC²-3 [15] code developed by the Argonne National Laboratory and the EXUS-F [16] code developed by Lim use this approach to generate multigroup cross-sections for fast reactor analysis, achieving good results in nuclear core criticality calculations, but their large computational costs are still unacceptable in shielding calculations.

The MATXS format is a widely used multigroup master library format for storing neutron and photon data that contains comprehensive cross-sections, group-to-group matrices, and other reaction data. TRANSX2.15 [17], developed by Los Alamos National Laboratory, is a cross-section processing code that can process multigroup neutron-photon coupled libraries in MATXS format to generate problem-dependent multigroup libraries in the ANISN format, GOXS format or other formats according to different realistic problems. Research shows [18] that there are still some restrictions with the TRANSX2.15, including (1) issues with processing cross-section libraries with fine group structures, such as the hyperfine library (640 groups); (2) issues with developing cross-sections with low background cross-sections (<0.1 b) for nuclides, such as ⁵⁶Fe; (3) difficulties in developing resonance self-shielding cross-sections for light nuclides, such as ¹²C and ¹⁶O. These issues are sure to pose a challenge to generating the high-precision, problem-dependent multigroup cross-sections, especially for some light nuclide shielding problems that produce fatal computational results. These issues must be resolved before the new problem-dependent multigroup macroscopic sections can be generated to obtain accurate shielding calculation results.

ARES [19] is a three-dimensional neutron-photon coupled transport shielding calculation code based on the S_N method, which can provide reliable transport results for shielding calculations of nuclear reactor devices. The multigroup neutron-photon macroscopic cross-section processing (MGMXS) module is independently developed to reduce

the multigroup cross-section errors in the shielding transport code ARES. Before using the MGMXS module, a multigroup cross-section library named EOS in MATXS format was developed. The module retrieves microscopic cross-sections from EOS and develops problem-dependent multigroup macroscopic cross-sections based on the material properties of the shielding problem. Then the working library in ANISN and ANISNB format can be produced to store these multigroup macroscopic cross-sections.

In the next section, a master library EOS in MATXS format is developed, and the theory and processing flow of the MGMXS module are introduced. Section 3 contains the numerical verification and result analysis, including the comparison of macroscopic cross-sections, self-designed problems, neutron-photon experiments and a fixed source shielding benchmark. The conclusions are presented in Section 4.

2. Methodology

2.1. The Pseudoproblem-Independent MATXS Library

The ENDF/B-VII.1 [20] evaluated nuclear data has been validated by numerous studies and is suitable for shielding calculations. The macroscopic cross-sections are problem-dependent and obtained through processing the multigroup master library with specific shielding problems. A multigroup neutron-photon coupled master library in MATXS format named EOS is provided from the ENDF/B-VII.1 evaluated nuclear data using the nuclear data processing code NJOY2016 [3]. The master library EOS includes multigroup neutron-photon coupled cross-sections for 202 nuclides commonly used in nuclear reactors. The library contains a large number of nuclides, which leads to low filling efficiency and a high error rate in NJOY2016 and BBC [11] input cards. We developed an automatic input card generation code that generates the required input cards with known nuclide numbers, reducing the time spent on the development of the MATXS library.

The master library EOS has a VITAMIN-B6 energy group structure with 199 groups for the neutron and 42 groups for the photon. This energy group structure (199 n + 42 γ) can be used for a variety of reactor designs and shielding problems, including thermal and fast reactor systems [21]. The resonance self-shielding of nuclides is the core of cross-section processing. KONNO [22,23] has demonstrated that the smallest background cross-section and weight flux of VITAMIN-B6 in AMPX format is not adequate, which will seriously affect the self-shielding correction. We selected appropriate parameters in generating the multigroup library EOS to consider these factors. The library contains data for 8 temperature points (300, 500, 700, 800, 900, 1400, 1800 and 2500 K) and 10 background cross sections (10^{10} , 10^5 , 10^4 , 10^3 , 3×10^2 , 10^2 , 50, 10, 1.0 and 0.1 b). By interpolating them, the real resonance cross-section of various nuclides can be considered. The neutron and photon cross-sections in the EOS are expanded by the P_8 order Legendre polynomial, including the 0~8 order scattering cross-sections, which can be used to calculate the strong anisotropic scattering problems. The neutron weighting function is of the form typically chosen for fission reactor shielding problems [24]. The neutron weight spectrum is composed of the smoothing function of Maxwell spectrum, $1/E$ spectrum, fast reactor energy spectrum and fission spectrum (weight spectrum parameter IWT = 8). The photon weight spectrum is composed of the smoothing function of $1/E$ spectrum with a roll-off at lower energies and a similar drop-off at higher energies (weight spectrum parameter IWT = 3). All the following transport calculations in this paper used the multigroup master library EOS.

2.2. Multigroup Macroscopic Cross-Section

2.2.1. Theory of Cross-Section Production

The main purpose of the module is to generate multigroup macroscopic cross-sections, such as total cross-section and scattering matrices, which is suitable for S_N calculations. The following describes how to generate these cross-section data. For simplicity, the steady-state transport equation in one-dimensional slab geometry takes the following form:

$$\mu \frac{\partial}{\partial z} \psi(z, E, \vec{\Omega}) + \Sigma_t(z, E) \psi(z, E, \vec{\Omega}) = \int_0^\infty dE' \int_{4\pi} \Sigma_s(z, E' \rightarrow E, \vec{\Omega}' \cdot \vec{\Omega}) \psi(z, E', \vec{\Omega}') d\vec{\Omega}' + q(z, E, \vec{\Omega}) \quad (1)$$

where $z, E, \vec{\Omega}$ are the spatial position, energy and direction; μ is the direction cosine of $\vec{\Omega}$; ψ is the angular flux; q is the fixed source term; Σ_t is macroscopic total cross-sections; Σ_s is macroscopic scattering cross-sections and can be expanded in the series of Legendre polynomials as Equation (2).

$$\Sigma_s(z, E' \rightarrow E, \mu_0) = \sum_{n=0}^{\infty} \frac{(2n+1)}{2} \Sigma_{s,n}(z, E' \rightarrow E) P_n(\mu_0) \tag{2}$$

where n is the order of the Legendre polynomial; $P_n(\mu)$ is the n -order Legendre polynomial. The next step is to substitute Equation (2) into Equation (1). Then, the multigroup P_N transport equation in 1D geometry is attained by integrating Equation (1) over a group g .

$$\mu \frac{\partial}{\partial z} \psi_g(z, \mu) + \sum_{n=0}^{\infty} \frac{2n+1}{2} P_n(\mu) \Sigma_{t,n,g}^{PN}(z) \phi_{n,g}(z) = \sum_{g'=1}^G \sum_{n=0}^{\infty} \frac{2n+1}{2} P_n(\mu) \Sigma_{s,n,g' \rightarrow g}^{PN}(z) \phi_{n,g'}(z) + q_g(z, \mu) \tag{3}$$

where the total cross-sections and scattering cross-sections are given by the following group average:

$$\Sigma_{t,n,g}^{PN}(z) = \frac{\int_g \Sigma_t(z, E) W_n(E) dE}{\int_g W_n(E) dE} \tag{4}$$

$$\Sigma_{s,n,g' \rightarrow g}^{PN}(z) = \frac{\int_{g'} dE' \int_g \Sigma_s(z, E' \rightarrow E) W_n(E) dE}{\int_g W_n(E) dE} \tag{5}$$

where $\phi_{n,g}(z)$ is the n -order, g -group flux moment and $W_n(E)$ are the weighting flux that should be chosen to be as similar to the true flux as possible. Then, the multigroup cross-section $\Sigma_{t,n,g}^{PN}(z), \Sigma_{s,n,g' \rightarrow g}^{PN}(z)$ can be generated by NJOY2016.

However, the multigroup transport equation solved by the S_N method is not directly equal to Equation (3), which requires appropriate deformation of Equation (3) to generate multigroup cross-sections. The collision term at the left of Equation (3) is moved to the right of the equation and combined with the scattering source term. At the same time, adding a new transport collision term $\Sigma_{t,g}^{S_N} \psi_g$ to both sides of the equation, the S_N transport equation is obtained by combining and simplifying.

$$\mu \frac{\partial}{\partial z} \psi_g(z, \mu) + \Sigma_{t,g}^{S_N}(z) \psi_g(z, \mu) = \sum_{g'=1}^G \sum_{n=0}^{\infty} \frac{2n+1}{2} P_n(\mu) \Sigma_{s,n,g' \rightarrow g}^{S_N}(z) \phi_{n,g'}(z) + q_g(z, \mu) \tag{6}$$

where

$$\begin{aligned} \Sigma_{s,n,g' \rightarrow g}^{S_N}(z) &= \Sigma_{s,n,g' \rightarrow g}^{PN}(z), g' \neq g \\ \Sigma_{s,n,g \rightarrow g}^{S_N}(z) &= \Sigma_{s,n,g \rightarrow g}^{PN}(z) - \Sigma_{t,n,g}^{PN}(z) + \Sigma_{t,g}^{S_N}(z), g' = g \end{aligned} \tag{7}$$

The $\Sigma_{t,g}^{S_N}$ in Equation (7) is not determined, so various transport approximations are used by choosing total cross-sections as Equation (8).

$$\begin{aligned} \text{Consistent - P} : \Sigma_{t,g}^{S_N}(z) &= \Sigma_{t,0,g}^{PN}(z) \\ \text{Inconsistent - P} : \Sigma_{t,g}^{S_N}(z) &= \Sigma_{t,N+1,g}^{PN}(z) \\ \text{Diagonal} : \Sigma_{t,g}^{S_N}(z) &= \Sigma_{t,N+1,g}^{PN}(z) - \Sigma_{s,N+1,g \rightarrow g}^{PN}(z) \\ \text{Extend} : \Sigma_{t,g}^{S_N}(z) &= \Sigma_{t,N+1,g}^{PN}(z) - \sum_{g'=1}^G \Sigma_{s,N+1,g \rightarrow g'}^{PN}(z) \end{aligned} \tag{8}$$

where N is the Legendre truncation order, indicating that P_N order of the Legendre expansion is used for shielding calculations.

In the resonance energy region, the neutron cross-sections appear as several resonance peaks and the resonance self-shielding effects of nuclides cannot be ignored. A simple technique called Bondarenko [25] method, based on the narrow resonance approximation, has high calculation efficiency and relatively satisfactory accuracy and is widely used to account for resonance self-shielding. Additionally, many studies found that this method has good adaptation to many other codes. Our module also implements this method to process and develop the resonance of the cross-sections. This method divides the total cross-section of material into two parts. One depends on the microscopic total cross-section and density of nuclide i only, and the other one depends on the total microscopic cross-section and density of all the nuclides in the material m except the nuclide i .

$$\Sigma_t^m(E) = N^i (\sigma_t^i(E) + \sigma_0^i) \quad (9)$$

where σ_0^i is called background cross-section,

$$\sigma_0^i = \frac{1}{N^i} \sum_{j \neq i} N^j \cdot \sigma_t^j(E) \quad (10)$$

The macroscopic cross-section of the shielding material m is calculated by summing the macroscopic cross-section of the individual nuclides.

$$\Sigma_{t,g}^m = \sum_{i \in m} N^i \sigma_{t,g}^i(T, \sigma_{0,g}^i) \quad (11)$$

The background cross-section for nuclide i cannot be obtained directly, and the initial background cross-section is usually obtained using an infinite dilution cross-section at nuclide temperature T . The true background cross-section for all nuclides is then generated using an interpolation-iterative method.

However, reactor shielding calculations contain complex geometric models and multiple material compositions. The effects of leakage must be considered by the addition of an effective escape cross-section, which is obtained by considering the geometry of a practical problem equal to the reciprocal of the mean chord length,

$$\sigma_{0,g}^i = \frac{1}{N^i} \left(\sum_{j \neq i}^M N^j \cdot \sigma_{t,0,g}^j(T, \sigma_{0,g}^j) + \frac{1}{l} \right) = \frac{1}{N^i} \left(\sum_{j \neq i}^M N^j \cdot \sigma_{t,0,g}^j(T, \sigma_{0,g}^j) + \frac{S}{4V} \right) \quad (12)$$

where S is the surface area of the lump and V is the volume of the lump.

2.2.2. The Cross-Section Processing Module

The calculation flowchart of MGMXS module is shown in Figure 1. It should be noted that the abbreviation "XS" in the flowchart means cross-sections. The nuclide information filled in by the user for each region on the input card is reorganized using a bubbling method, and then microscopic cross-sections are retrieved from the MATXS library with the aim of saving memory and improving computational efficiency. The resonance cross-sections of the nuclide are dependent on temperature and background cross-sections and need to be generated by an interpolation-iteration method. During the iteration process, linear interpolation is used for temperature, while the logarithm of the background cross-section is first calculated, and then linear interpolation is used. The linear interpolation method is stable and reliable, does not result in non-physical oscillations and ensures that the total cross-sections and the sum of the cross-sections of each reaction type are equal. Meanwhile, the neutron scattering is divided into elastic and inelastic scattering. The elastic scattering cross-section is considered in resonance calculations. The inelastic scattering cross-section, which does not vary with the background cross-section, does not require resonance processing, thus reducing the computational cost of resonance self-shielding calculations.

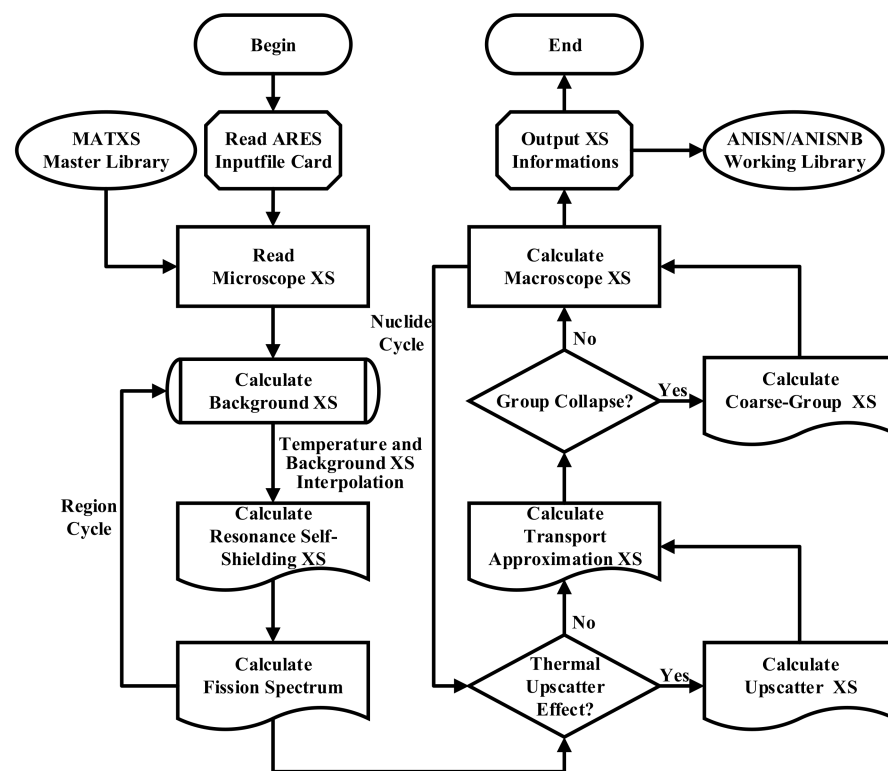


Figure 1. Flowchart of MGMXS module framework.

Moreover, the MGMXS module also develops multiple modules to generate neutron fission cross-sections, fission spectrum, transport cross-sections and up scatter cross-sections to address various types of calculation problems. The module also applies a simple group collapse method that uses the scalar flux as the weighting function to generate coarse cross-sections. The scalar flux can be obtained by 1D transport calculation. After processing these, microscopic cross-sections of all nuclides can be obtained. The postprocessing module generates macroscopic cross-section tables for each region and outputs ANISN and ANISNB libraries for S_N transport codes. MGMXS module, in contrast to TRANSX2.15, can output the required reaction type and microscopic cross-sections of nuclides for specific types of calculations, such as burnup calculations. The photon is combined with the neutron in the neutron-photon coupled problems, and it is the additional group of the neutron in the low energy region.

3. Numerical Verification and Result Analysis

3.1. Homogeneous Mixed-Medium Cross-Section Comparison

A homogeneous mixed medium was used to test the correctness of the development of the MGMXS module. Uranium is the main component material of the core, and 3.3% enriched ^{235}U was used as the test material. The true background cross-sections were generated through interactions. ^{235}U and ^{238}U are both fission isotopes with their own fission spectrum. Here, the mixed fission spectrum of the medium is calculated. The background cross-sections, total cross-sections, neutron production cross-sections and fission spectrum of the medium were obtained using the MGMXS module and TRANSX2.15, and the relative difference of both two codes is shown in Figures 2–5.

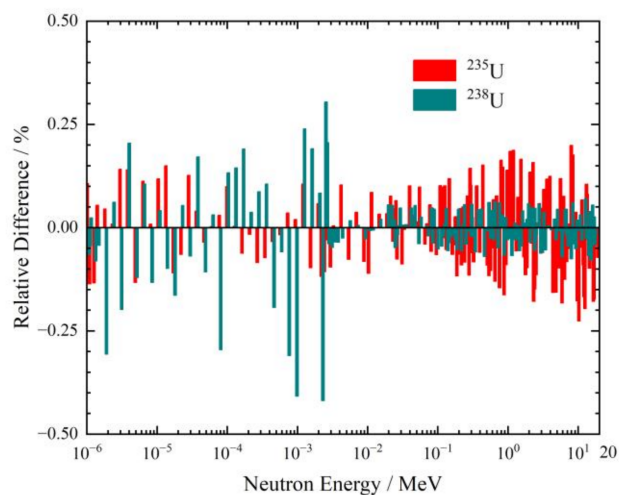


Figure 2. The relative differences of background cross-sections.

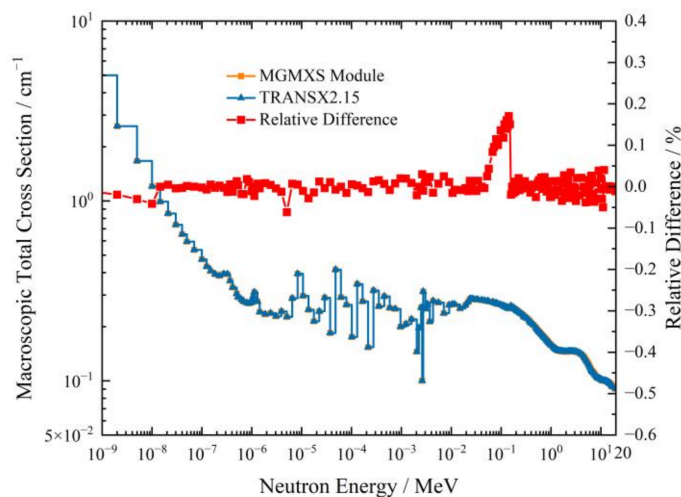


Figure 3. The relative differences of macroscopic total cross-sections.

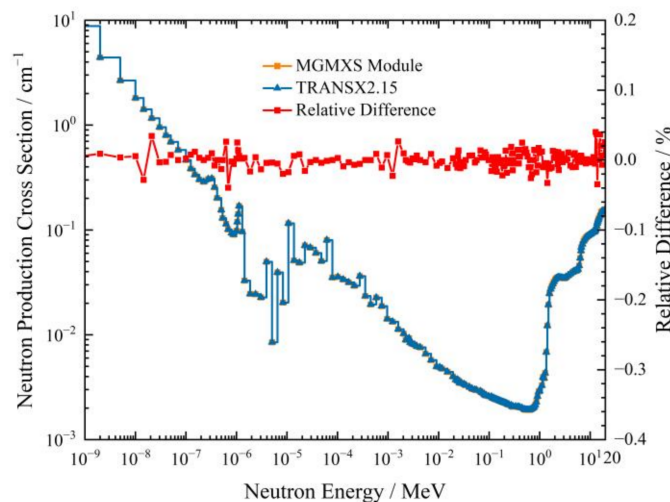


Figure 4. The relative differences of neutron production cross-sections.

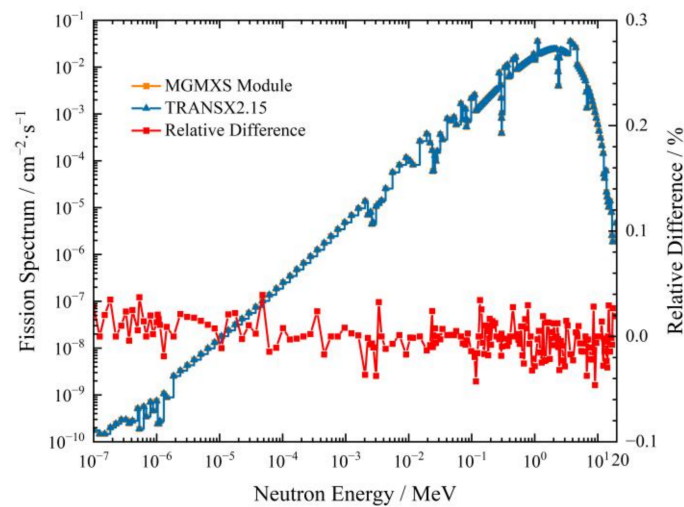


Figure 5. The relative differences of fission spectrum.

Figure 2 displays the relative differences of the background cross-sections that exist between the two codes. In most neutron energy regions, the relative differences are less than 0.2% for both ^{235}U and ^{238}U . In the middle energy region, the relative differences of ^{238}U exist with some large values, but the maximum does not exceed 0.5%. The background cross-sections of the MGMXS module and TRANSX2.15 show good agreement, which confirms the capability to accurately calculate the background cross-sections by the MGMXS module.

Figures 3 and 4 show that the calculation results of the total cross-section and neutron production cross-section of the two codes are basically the same, and the relative differences are all less than 0.2%. Figure 5 shows that the relative differences in the mixed fission spectrum are less than 0.1%. The errors are attributed to the different effective numbers of cross-sections resulting from the distinct data output formats of the MGMXS module and the TRANSX2.15. Overall, the MGMXS module shows good calculation accuracy for both the cross-sections and fission spectrum.

3.2. Self-Designed Problem and Experiment Verification

The self-designed problems with a single nuclide and a series of experiments, including ALARM-CF-FE-SHIELD-001 [26] and OKTAVIAN [27], were chosen to verify the accuracy of the cross-sections generated by the MGMXS module in shielding problems. ANISN [28], which is an international common 1D S_N transport code and widely used for multigroup cross-section verification and shielding calculations, was used for all transport calculations in this section. This code was chosen due to its high computational efficiency and for not introducing additional physical uncertainties, thus ensuring reliable results. The problem-dependent multigroup macroscopic cross-section is provided by the MGMXS module and TRANSX2.15 according to the self-designed problems and experimental data.

3.2.1. Self-Designed Problem with a Single Nuclide

The self-shielding correction for light nuclides in the official release of TRANSX2.15 has some difficulties, which can result in errors in P_0 expansion in-group scattering cross-section data and lead to a large neutron flux. A self-designed one-dimensional problem was utilized to test the capability of the MGMXS module to handle these self-shielding correction effects. The geometric model of the self-designed problem is shown in Figure 6. The model consists of a sphere of 100 cm in radius with an isotropic neutron source of 17.32–19.64 MeV at the center. The material of the sphere includes graphite, oxygen, aluminum and iron (^{12}C , ^{16}O , ^{27}Al , and ^{56}Fe), and the same material was used for the shielding shell. Multigroup macroscopic cross-sections were produced by the MGMXS module and TRANSX2.15. The results obtained from the MCNP [29] code, utilizing continuous-energy nuclear data, were used as a reference.

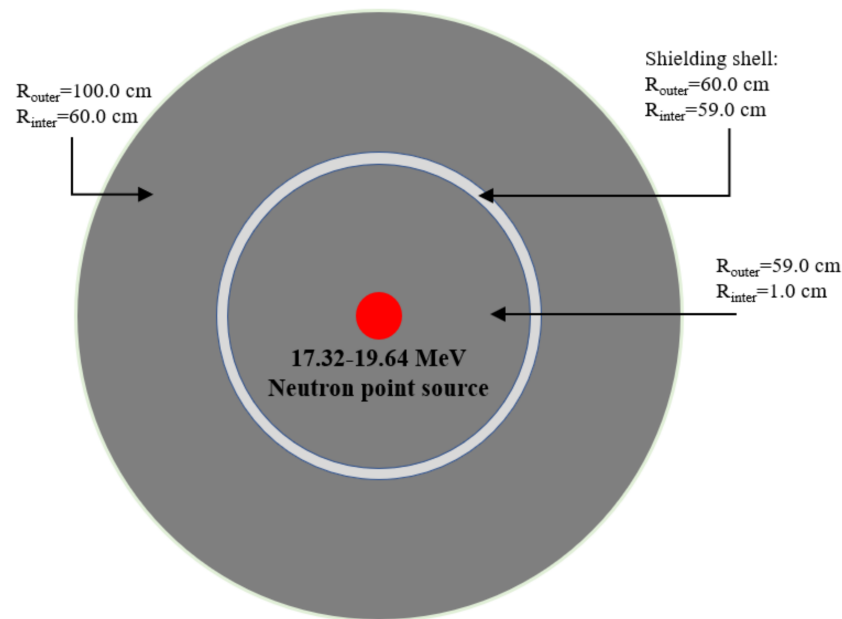


Figure 6. Geometric diagram of the self-designed one-dimensional sphere model.

The neutron spectrum calculation results for the four single nuclide self-designed problems at the 59.0–60.0 cm spherical shell are shown in Figure 7. The MGMXS module, TRANSX2.15 and MCNP calculations above 10 MeV show good agreement for the ^{12}C and ^{16}O , with TRANSX2.15 exhibiting larger differences as energy decreases. TRANSX2.15 still has a small difference from the reference values for the ^{27}Al . The reason for this difference is that TRANSX2.15 has difficulty processing the self-shielding correction for these nuclides [18]. The maximum number of scattering groups in TRANSX2.15 is set to five, which is insufficient to describe the neutron scattering of 199 groups during the self-shielding correction calculation. The self-shielding correction influence diminishes as the atomic number of the nuclide rises, such as ^{27}Al and ^{56}Fe . The MGMXS module employs a new method to determine the number of scattering groups automatically and prevent issues, such as TRANSX2.15, which allocates memory data in accordance with the scattering range of the nuclide in the MATXS library.

Both the TRANSX2.15 and MGMXS module calculated results are consistent with the reference values for the ^{56}Fe . This comparison shows that both codes have similar capabilities in resonance self-shielding correction, indicating that either code could accurately model systems containing nuclides with atomic numbers similar to ^{56}Fe .

The results of TRANSX2.15 without self-shielding correction were calculated to demonstrate this self-shielding correction effect, as shown in Figure 8. The calculation results of ^{12}C and ^{16}O were improved significantly, and they were in good agreement with the MGMXS module and the reference values. Nevertheless, TRANSX2.15 failed to account for the resonance self-shielding effect for ^{27}Al and ^{56}Fe , which caused the cross-section to deviate from real data and, as a result, produce inconsistent results in resonance energy groups. On the other hand, the calculation results of the four nuclides using the MGMXS module were consistent with the reference values, indicating that the MGMXS module can handle the self-shielding correction of the nuclides correctly.

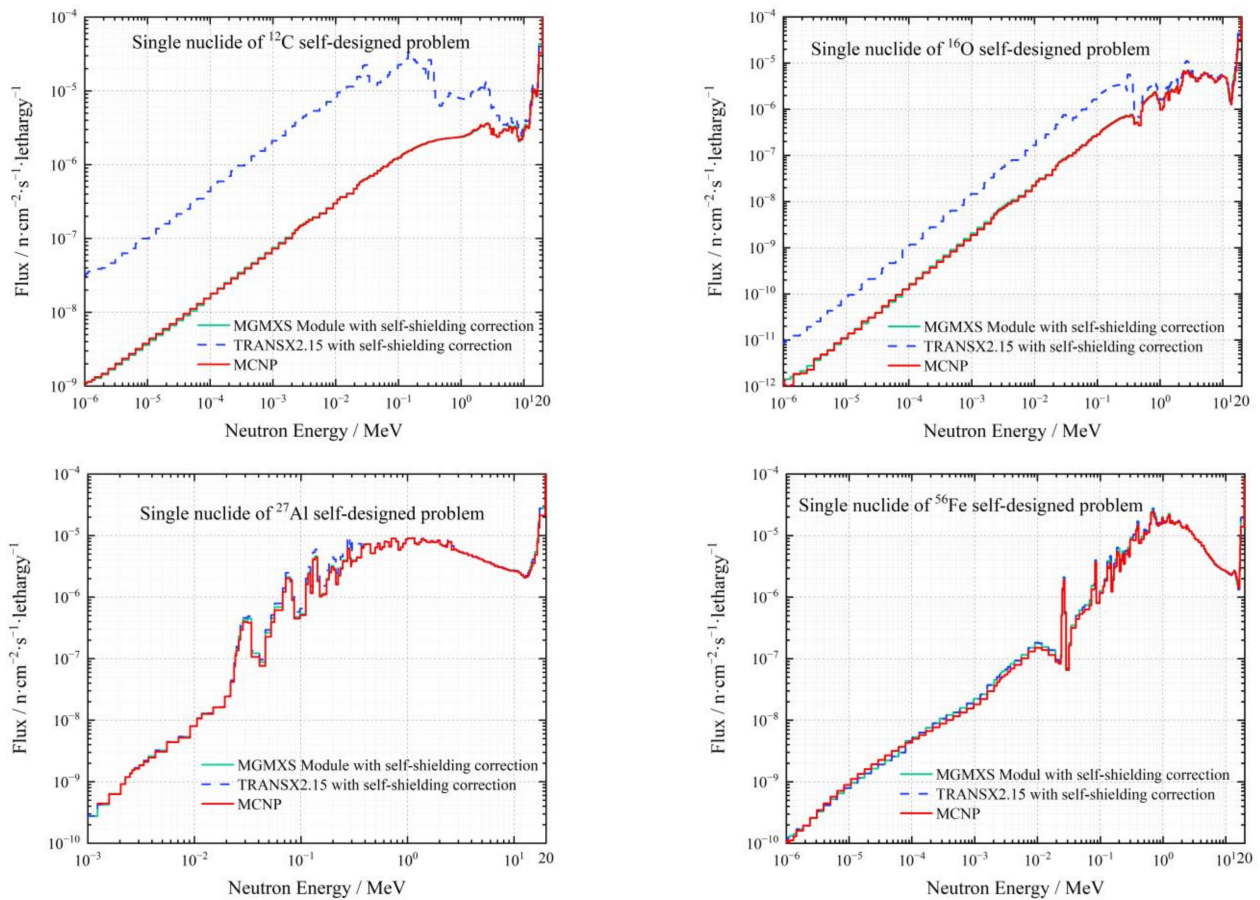


Figure 7. Comparison of self-designed problems with self-shielding correction.

3.2.2. ALARM-CF-FE-SHIELD-001 Experiment

The ALARM-CF-FE-SHIELD-001 experiment, as shown in Figure 9, was conducted at the IPPE in 1980. The experiment used the time-of-flight (TOF) method to study the neutron leakage spectrum of iron spheres of different diameters (Radii = 10, 15, 20, 25, 30 and 35 cm). The iron sphere is modeled with a ²⁵²Cf point source at its center, and the outside region is composed of iron shielding material. The detectors are located outside the iron sphere, with an outer radius that is three times the radius of the iron sphere.

The results of the neutron leakage spectrum for iron spheres with radii of 10, 20, 30 and 35 cm are shown in Figure 10. The differences between the MGMXS module and TRANSX2.15 calculation results are small, indicating that the calculation accuracy of the MGMXS module is comparable to that of TRANSX2.15. The neutron leakage spectrum results showed good agreement with the experimental data in the high-energy region, falling within the experimental error. There is a slight discrepancy in the low-energy region, which can be attributed to the difference in energy group structures used in the calculations and the experiment. Therefore, it is recommended to use energy group structures that are as similar as possible to those used in the experiment for future comparisons. Overall, the calculation results demonstrate good prediction of the neutron leakage spectrum of the iron sphere.

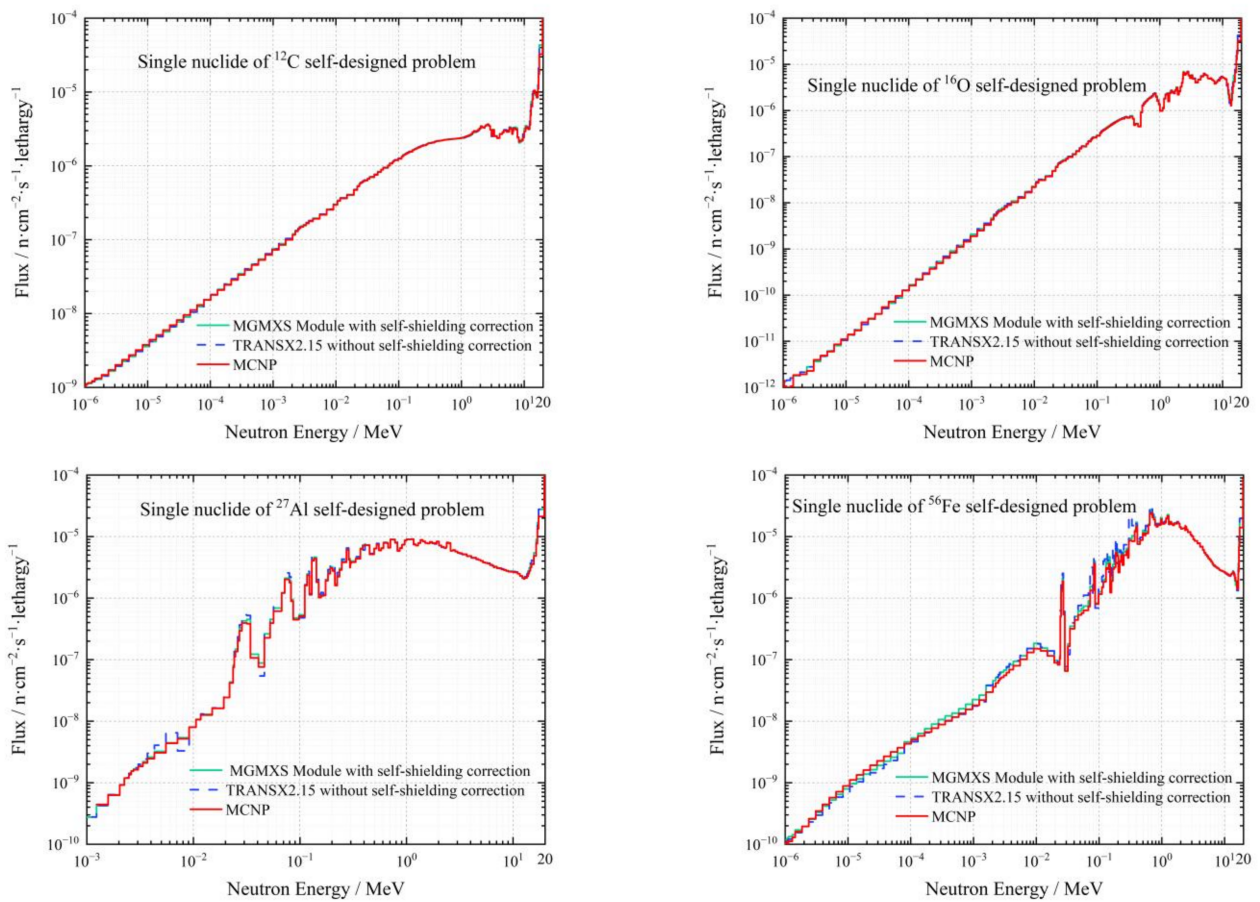


Figure 8. Comparison of self-designed problems without self-shielding corrections.

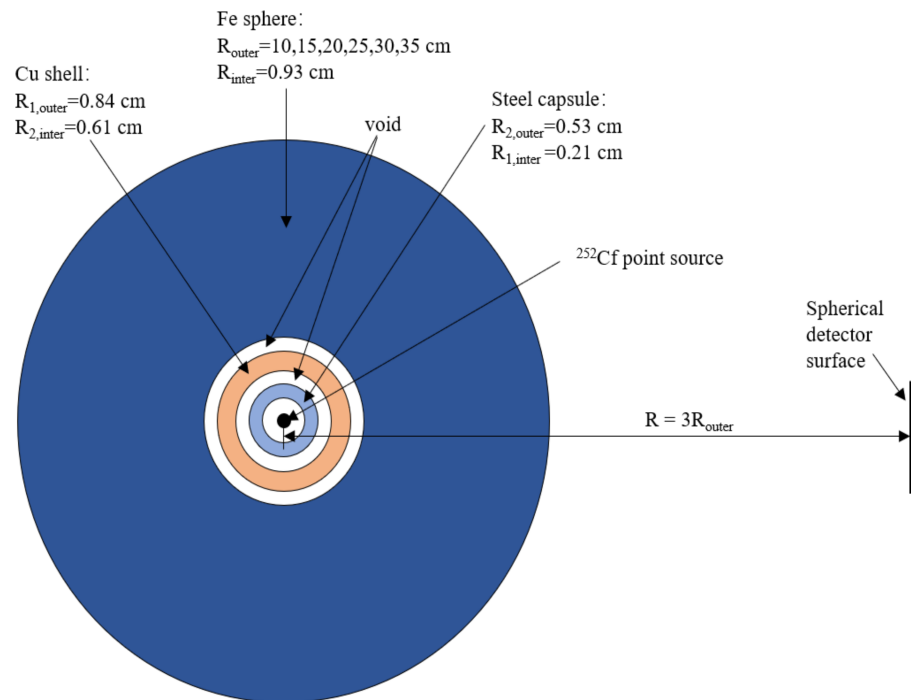


Figure 9. Geometry model of the ALARM-CF-FE-SHIELD-001 experiment.

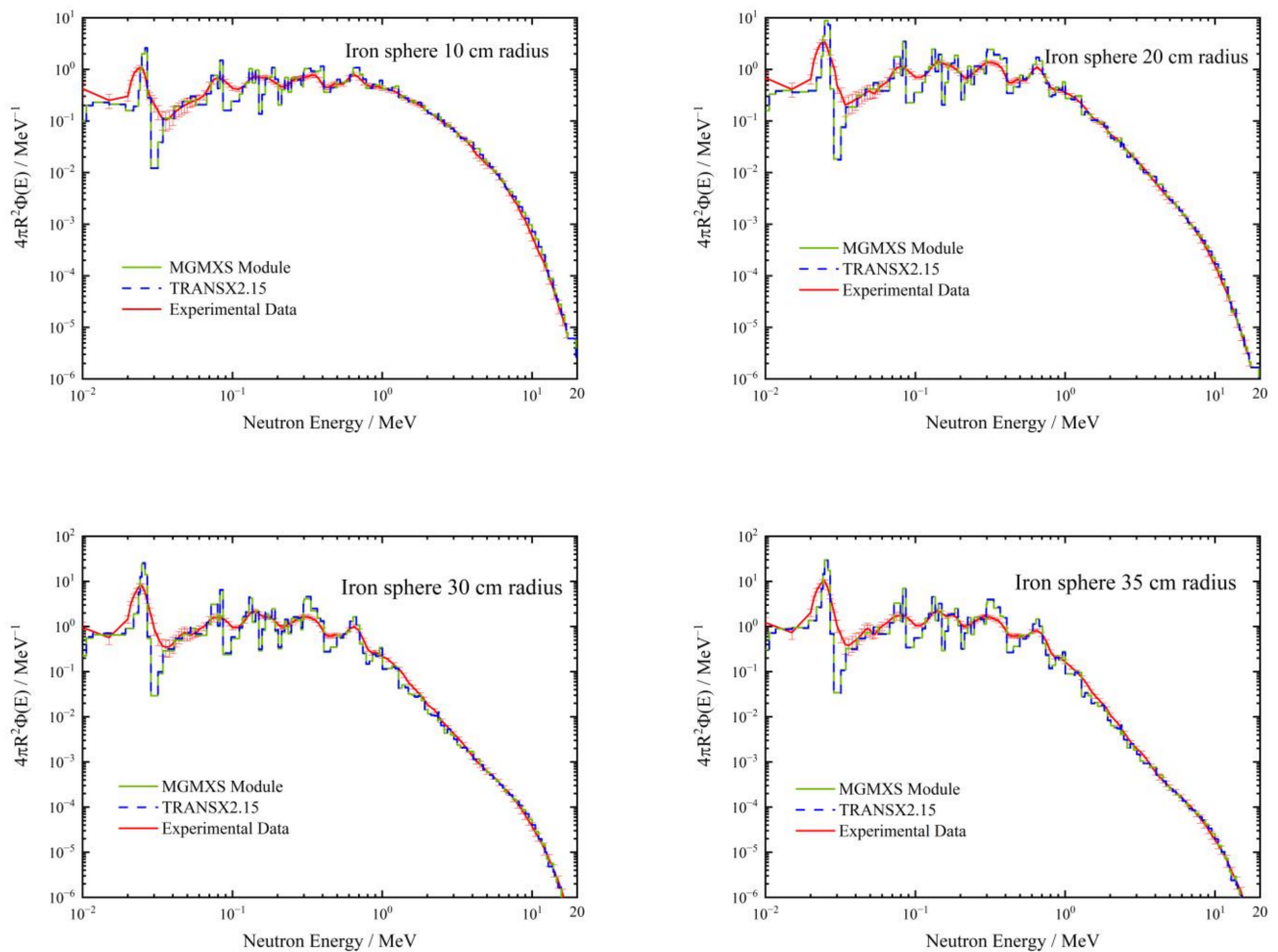


Figure 10. Comparison of experimental and calculated results of different radii of iron sphere.

3.2.3. OKTAVIAN Benchmark Experiment

The OKTAVIAN device is a 14 MeV D-T neutron source facility located at Osaka University. Between 1984 and 1988, researchers employed the TOF method to measure the neutron and γ leakage spectrum of various spherical shell materials, including Si, Al, W, Cu, Mo, Co, Nb, Pb, etc. An NE-218 scintillation detector was used to measure the neutron leakage spectrum from 0.1 MeV to 14 MeV. An NaI scintillator detector was used to measure the photon leakage spectrum. Notably, with the exception of Pb material, the γ and neutron experiments had the same geometry and neutron source. Transport calculations were able to simultaneously obtain both neutron and γ leakage spectra results.

The neutron leakage spectrum of OKTAVIAN-Al, OKTAVIAN-Si, OKTAVIAN-W and OKTAVIAN-Cu were calculated, as shown in Figure 11. The multigroup macroscopic cross-sections were generated using the MGMXS module and TRANSX2.15, respectively. The neutron leakage spectrum results from both codes are basically the same for these four experiments. The calculated results are in good agreement with the experimental data in most energy groups. There are some errors between the calculated results and the experimental data in some energy groups. Researchers at Mohammed V University [30] used the MCNP code and the ENDF/B-VII.1 evaluated nuclear data library to calculate the series of OKTAVIAN experiments, and similar errors were observed in the same energy regions between their calculation results and experimental data. Our calculation results show a similar trend to theirs, and the reason for the errors may be due to the lack of accuracy in the evaluated nuclear data libraries.

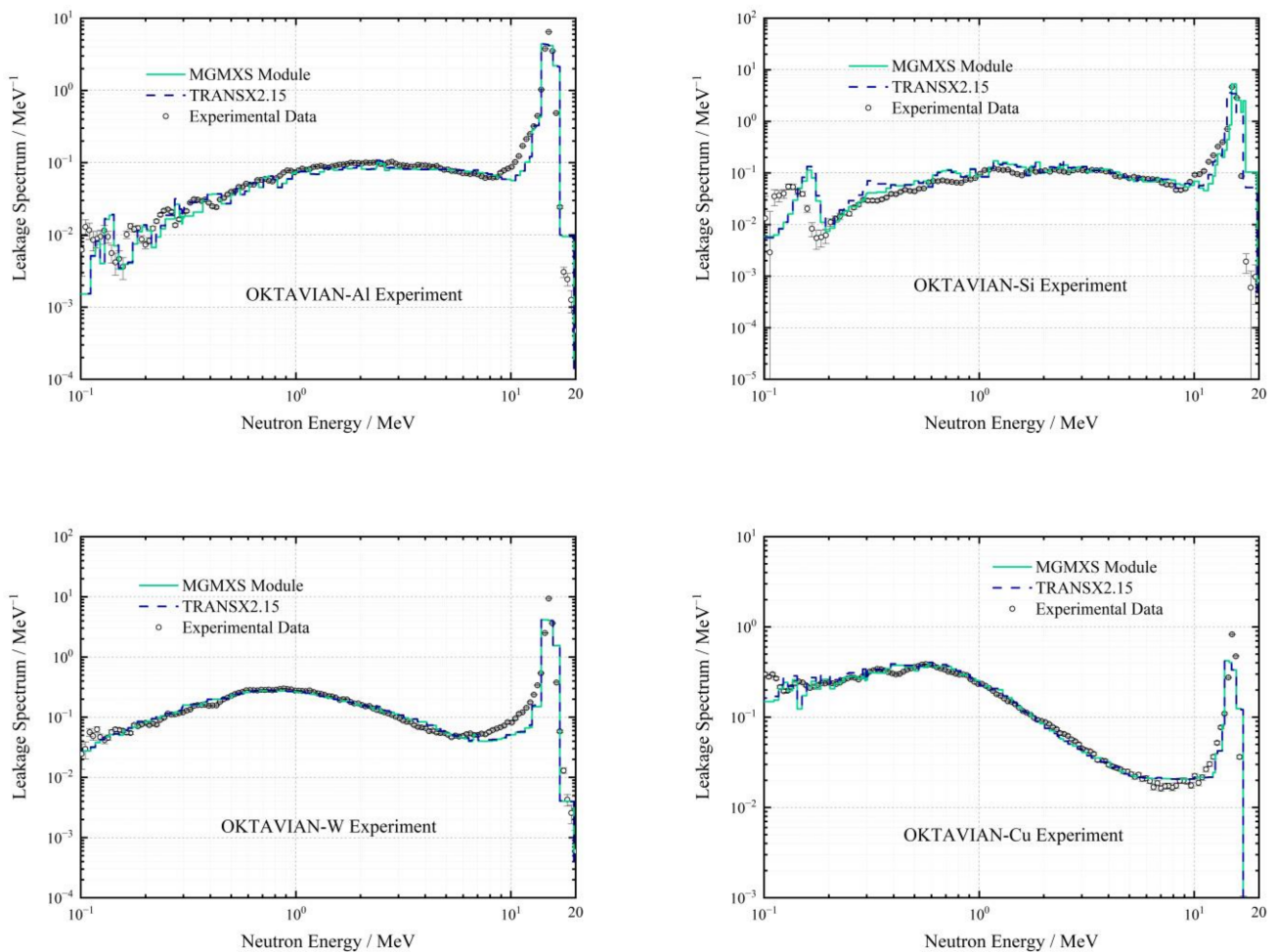


Figure 11. Comparison of experimental and calculated results of neutron leakage spectrum.

The photon leakage spectrum of the four series of OKTAVIAN experiments (OKTAVIAN-Al, OKTAVIAN-Si, OKTAVIAN-W and OKTAVIAN-Cu) was calculated to verify the accuracy of the photon cross-sections generated by the MGMXS module, and the results are shown in Figure 12. The photon leakage spectrum results from the MGMXS module and TRANSX2.15 are basically the same for these four experiments. The results from both codes show similar trends to the experimental data. However, both results of the two codes exhibit a peak at 0.511 MeV due to the electron annihilation effect, leading to an error compared to the experimental data. Nevertheless, the differences between the results of these two codes are small, and the accuracy of the generated photon cross-sections is comparable.

3.3. Fixed Source Benchmark Verification

3.3.1. JANUS Phase I Benchmark

The JANUS Phase I benchmark was selected to verify the applicability of the multi-group cross-section processing module in actual engineering shielding problems and the accuracy of the problem-dependent multigroup macroscopic cross-section generated by this module. The JANUS Phase I benchmark is completing the UK shielded installation ASPIS, connecting to the NESTOR light water moderated reactor, where thermal neutrons are slowed down by graphite and drive a natural uranium conversion target that serves as the neutron source for the experiment. The purpose of the experiment is to test the prediction of neutron penetration through stainless steel when the incident spectrum is typical of that emerging from a fast reactor. Figure 13 shows the JANUS Phase I computational model, which consists of 16 slabs of steel with a cavity area of 0.84 cm between the plates for the

threshold detectors. The first four plates are 17.85 cm thick mild steel to ensure that the neutron spectrum is the fast reactor energy spectrum. The middle nine plates are 40.39 cm thick stainless steel, which is the experimental area for the benchmark. The last three plates are 56.72 cm thick mild steel.

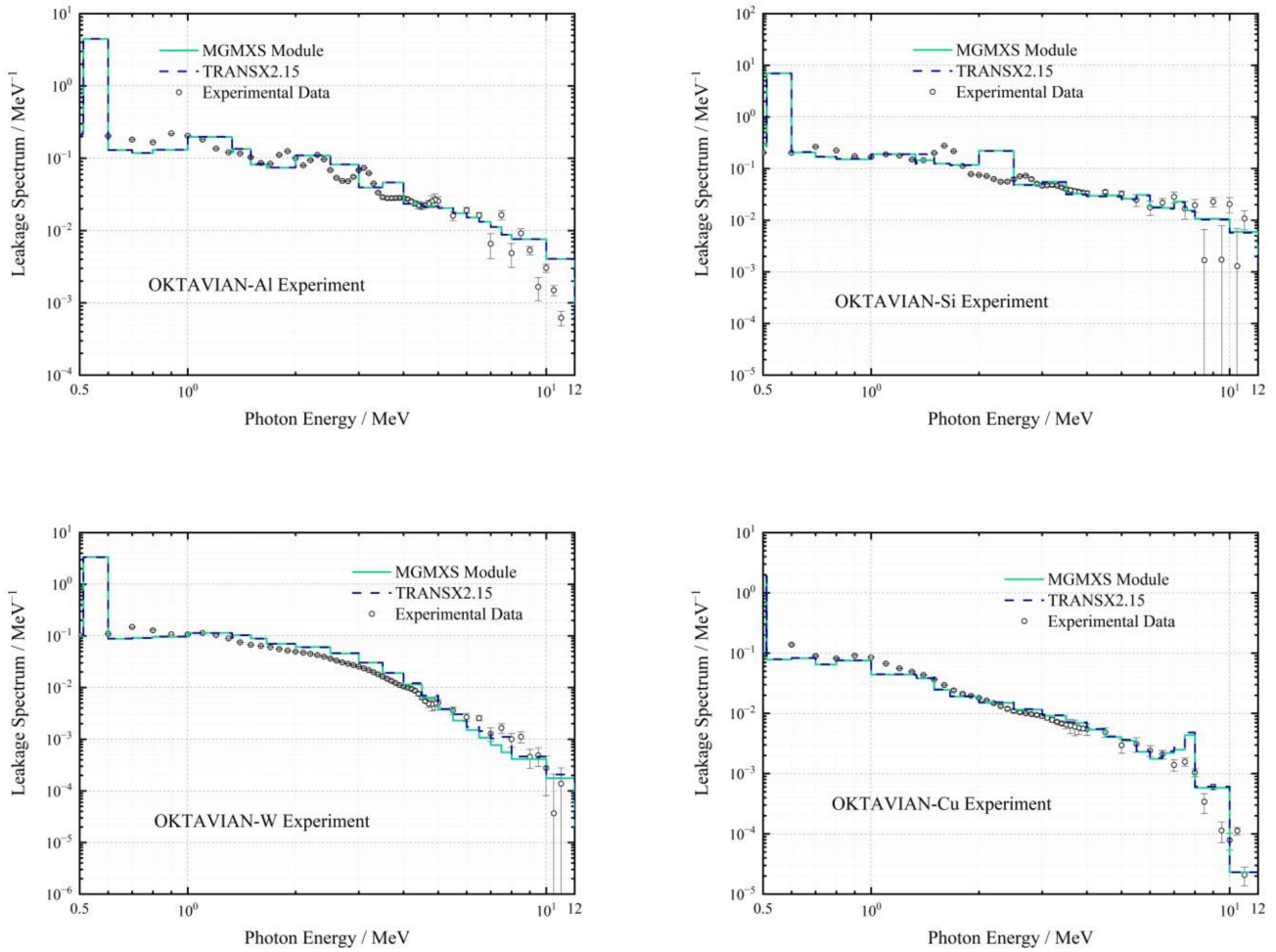


Figure 12. Comparison of experimental and calculated results of photon leakage spectrum.

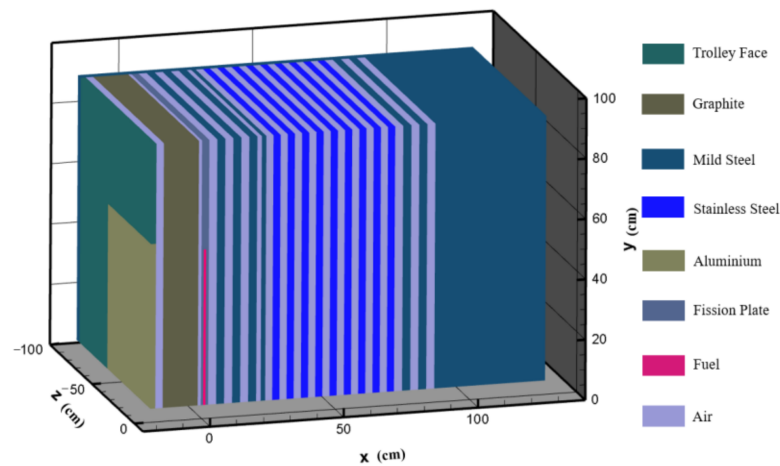


Figure 13. Computational model of the JANUS Phase I benchmark.

3.3.2. Calculation Results

The threshold detectors are placed along the axis of the model centerline to measure the reaction rates, including the following responses: $^{32}\text{S}(n,p)^{32}\text{P}$ and $^{103}\text{Rh}(n,n')^{103\text{m}}\text{Rh}$. The detector response cross-section data were obtained from the IRDFF-II library [31], and averaged cross-sections were used for different boundaries. The problem-dependent multigroup macroscopic cross-sections are generated by the macroscopic cross-section processing module, using a 199-group neutron energy structure and performing separate resonance self-shielding corrections based on the physical properties of materials in different regions. The shielding transport code ARES was used for the transport calculations. The reaction rate results obtained from calculations and experiments for the $^{103}\text{Rh}(n,n')^{103\text{m}}\text{Rh}$ and $^{32}\text{S}(n,p)^{32}\text{P}$ detectors are shown in Figure 14.

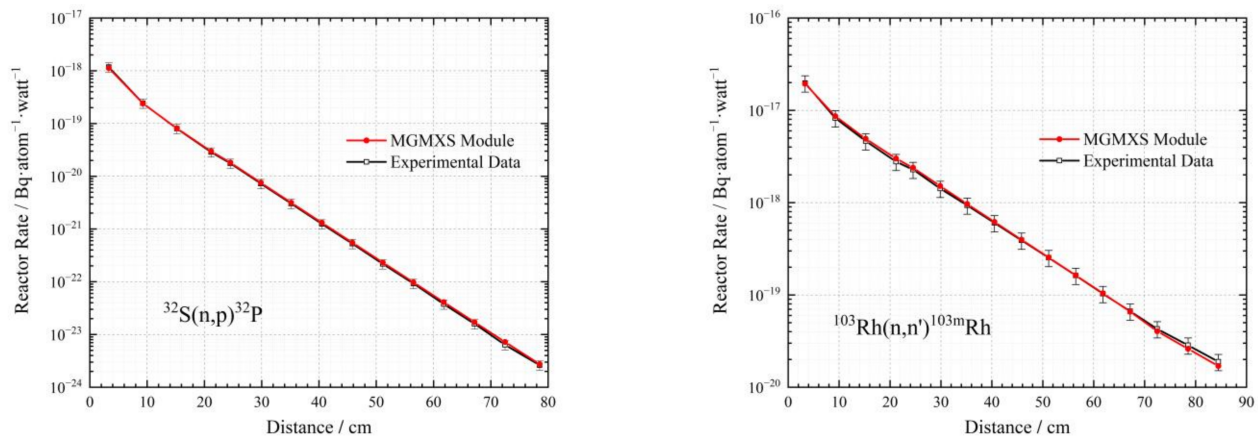


Figure 14. The reaction rate results of detectors for the JANUS Phase I benchmark.

Firstly, the reaction rates of both $^{32}\text{S}(n,p)^{32}\text{P}$ and $^{103}\text{Rh}(n,n')^{103\text{m}}\text{Rh}$ detectors decreased with increasing geometric depth at a nearly constant rate of decrease. The reaction rate of the $^{32}\text{S}(n,p)^{32}\text{P}$ detector decreased faster than that of the $^{103}\text{Rh}(n,n')^{103\text{m}}\text{Rh}$ detector. The reaction rate of the $^{32}\text{S}(n,p)^{32}\text{P}$ detector decreased by approximately six orders of magnitude at a depth of 80 cm, while that of the $^{103}\text{Rh}(n,n')^{103\text{m}}\text{Rh}$ detector decreased by three orders of magnitude. The reason is that as the distance increases, many fast neutrons are slowed down and their energy decreases. However, the reaction threshold of the $^{32}\text{S}(n,p)^{32}\text{P}$ detector is approximately 1.0 MeV, while that of the $^{103}\text{Rh}(n,n')^{103\text{m}}\text{Rh}$ detector is approximately 0.04 MeV. The slowed-down neutrons are more capable of activating the $^{103}\text{Rh}(n,n')^{103\text{m}}\text{Rh}$ detector.

Then, the calculation results of the $^{32}\text{S}(n,p)^{32}\text{P}$ detector agree well with the experimental data, with relative errors mostly within $\pm 10\%$. There is a 15% overestimation at the 72.5 cm position, which may be attributed to the evaluated nuclear data of the nuclides [32], indicating that further improvements are necessary. The relative errors for the $^{103}\text{Rh}(n,n')^{103\text{m}}\text{Rh}$ detector are also within $\pm 10\%$. Overall, the relative errors between the calculated and experimental results for the JANUS Phase I benchmark are within $\pm 20\%$, which meets the requirements of shielding calculations and verifies the accuracy of the macroscopic cross-sections generated by the MGMXS module in engineering shielding problems.

4. Conclusions

The multigroup neutron-photon macroscopic cross-section processing module was independently developed in the shielding transport code ARES to meet the accuracy requirements for 3D shielding calculations. The module can read the neutron-photon coupled master library in MATXS format, process and develop problem-dependent multigroup macroscopic cross-sections of neutrons and photons tailored to shielding calculations and generate working libraries in various formats for S_N transport codes. The correctness and

accuracy of the MGMXS module was verified for macroscopic cross-section comparison, self-designed problems and a series of shielding experiments. The applicability of this module to engineering problems was tested for a fixed-source shielding benchmark.

The macroscopic total cross-sections, background cross-sections, neutron production cross-sections, and fission spectrum produced by the MGMXS module show good agreement with TRANSX2.15. For the self-designed problems with a single nuclide, TRANSX2.15 has difficulties in dealing with resonance self-shielding correction for light nuclides (such as ^{12}C and ^{16}O) and differs significantly from the reference values. In contrast, the MGMXS module has no such difficulties, and the calculated results are in good agreement with the reference values, correctly handling resonance self-shielding correction for light nuclides. For the shielding experiments, the neutron leakage spectrum for a series of experiments was calculated, including ALARM-CF-FE-SHIELD-001 and OKTAVIAN. The neutron leakage spectrum results from the MGMXS module and TRANSX2.15 were consistent with the experimental data. The photon leakage spectrum for the four series of OKTAVIAN experiments was also calculated, and the differences between the calculated results of the two codes and the experimental data were relatively small. The JANUS Phase I fixed source shielding benchmark shows that the reaction rate calculation results from the MGMXS module had relative differences from the experimental data within $\pm 20\%$, meeting the accuracy requirements for shielding calculations.

Although the results of the MGMXS module show good agreement with TRANSX2.15 and have improved the self-shielding correction, some errors still exist when compared to the reference values due to the differences in energy group structure and the accuracy of the evaluated nuclear data. Moreover, the usability of the module in engineering shielding problems has only been preliminarily verified, and more actual benchmark experiments are needed for comparison. Currently, the MGMXS module uses the Bondarenko method based on the narrow resonance approximation to handle the resonance self-shielding correction, which can accurately describe the unresolved resonance regions. However, as for the resolved resonance regions, there are some resonance peaks that cannot be accurately described by the narrow resonance approximation, which will introduce uncertainties into the transport calculations. The accurate treatment for the resolved resonance regions remains an open problem. Especially for the new reactor types such as research and fusion reactors, as the geometry and structure of the device become more complex and the size of the model increases, the physical characteristics will differ from those of PWRs. The accuracy of multigroup cross-sections is required to be increased for shielding calculations, and the applicability of the multigroup macroscopic cross-sections generated by the current methods still needs further research.

Author Contributions: Conceptualization, X.Z.; methodology, X.Z. and J.W.; software, X.Z.; validation, X.Z. and W.X.; formal analysis, X.Z.; investigation, W.X. and J.H.; data curation, X.Z.; writing—original draft preparation, X.Z.; writing—review and editing, B.Z. and S.S.; supervision, S.S. and J.H.; project administration, B.Z.; funding acquisition, B.Z. and S.S. All authors have read and agreed to the published version of the manuscript.

Funding: This research was funded by the Key Laboratory of Nuclear Data foundation, JCKY2022201C156.

Data Availability Statement: Not applicable.

Conflicts of Interest: The authors declare no conflict of interest.

References

1. Zhang, L.; Jia, M.C.; Gong, J.J.; Xia, W.M.; Chen, J.J. Overview of calculation methods and codes for reactor radiation shielding. *Nucl. Electron. Detect. Technol.* **2018**, *38*, 516–520.
2. Lewis, E.; Miller, W. *Computational Methods of Neutron Transport*; Wiley: Hoboken, NJ, USA, 1984.
3. MacFarlane, R.E. *The NJOY Nuclear Data Processing System Version 2016*; La-UR-17-20093; U.S. Department of Energy Office of Scientific and Technical Information: Oak Ridge, TN, USA, 2016.
4. Wiarda, D.; Williams, M.L.; Celik, C.; Dunn, M.E. *Ampx: A Modern Cross Section Processing System for Generating Nuclear Data Libraries*; Oak Ridge National Lab. (ORNL): Oak Ridge, TN, USA, 2015.

5. Xu, N.; Zu, T.; Cao, L.; Wu, H. Development of the capability for multi-group shielding library generation in the nuclear data processing code NECP-Atlas. *Ann. Nucl. Energy* **2022**, *173*, 109125. [CrossRef]
6. Manturov, G.N.; Nikolaev, M.N.; Tsiboulia, A.M. Group Constant System ABBN-93. Part 1: Nuclear Constants for Calculation of Neutron and Photon Emission Fields. In *Issues of Atomic Science and Technology: Russian*; International Atomic Energy Agency (IAEA): Vienna, Austria, 1996.
7. White, J.E. *Production and Testing of the VITAMIN-B6 Fine-Group and the BUGLE-93 Broad-Group Neutron/Photon Cross-Section Libraries Derived from ENDF/B-VI.3 Nuclear Data*; Oak Ridge National Lab: Oak Ridge, TN, USA, 2001.
8. Grabeznoy, V.; Koshcheev, V.; Lomakov, G.; Manturov, G. Verification of the ABBN-RF2010 constants in calculations of shielding benchmarks. *Prog. Nucl. Sci. Technol.* **2014**, *4*, 587–590. [CrossRef]
9. Chen, Y.X.; Chen, C.B.; Wu, J.; Yang, S.H.; Lu, D.G. Verification and validation of multi-group library MUSE1.0 created from ENDF/B-VII.0. *Nucl. Power Eng.* **2010**, *31*, 6–10.
10. Kim, D.H.; Gil, C.S.; Lee, Y.O. Validation of an ENDF/B-VII.0-based neutron and photon shielding library in MATXS-format. *J. Korean Phys. Soc.* **2011**, *59*, 1199. [CrossRef]
11. Radiation Safety Information Computational Center. *Doors3.2: One-, Two- and Three-Dimensional Discrete Ordinates Neutron/Photon Transport Code System*; CCC-650; Oak Ridge National Lab: Oak Ridge, TN, USA, 1998.
12. Ilas, G.; Hiscox, B. *Validation of SCALE 6.2.4 and ENDF/B-VII.1 Data Libraries for Nuclide Inventory Analysis in PWR Used Fuel*; Oak Ridge National Lab: Oak Ridge, TN, USA, 2021.
13. Manturov, G.N.; Nikolaev, M.N.; Poljakov, A.J.; Tsibulya, A.M. *Notes on the CONSYST Code*; No. INDC (CCP)-426; International Atomic Energy Agency (IAEA): Vienna, Austria, 2001.
14. Nguyen, T.D.C.; Lee, H.; Lee, D. Use of monte carlo code mcs for multigroup cross section generation for fast reactor analysis. *Nucl. Eng. Technol.* **2021**, *53*, 2788–2802. [CrossRef]
15. Lee, C.; Yang, W.S. MC²-3: Multigroup cross section generation code for fast reactor analysis. *Nucl. Sci. Eng.* **2017**, *187*, 268–290. [CrossRef]
16. Lim, C.; Joo, H.G.; Yang, W.S. Development of a fast reactor multigroup cross section generation code EXUS-F capable of direct processing of evaluated nuclear data files. *Nucl. Eng. Technol.* **2018**, *50*, 340–355. [CrossRef]
17. MacFarlane, R.E. TRANSX 2.15: A Code for Interfacing MATXS Cross-Section Libraries to Nuclear Transport Codes. 1998. Available online: <https://sgp.fas.org/othergov/doe/lanl/lib-www/la-pubs/00193527.pdf> (accessed on 2 April 2021).
18. IAEA Nuclear Data Section. *FENDL Library for Fusion Neutronics Calculations*; International Atomic Energy Agency (IAEA): Vienna, Austria, 2018.
19. Zhang, L.; Zhang, B.; Liu, C.; Zheng, J.; Zheng, Y.; Chen, Y. Calculation of the C5G7 3-D extension benchmark by ARES transport code. *Nucl. Eng. Des.* **2017**, *318*, 231–238. [CrossRef]
20. Chadwick, M.B.; Herman, M.; Obložinský, P.; Dunn, M.E.; Danon, Y.; Kahler, A.C.; Smith, D.L.; Pritychenko, B.; Arbanas, G.; Arcilla, G.; et al. ENDF/B-VII. 1 nuclear data for science and technology: Cross sections, covariances, fission product yields and decay data. *Nucl. Data Sheets* **2011**, *112*, 2887–2996. [CrossRef]
21. Kim, D.H.; Gil, C.S.; Kim, J.D.; Chang, J. Generation and validation of a shielding library based on ENDF/B-VI. 8. *Radiat. Prot. Dosim.* **2005**, *115*, 232–237. [CrossRef]
22. Konno, C. *Some Comments on JSSTD-300*; (No. JAERI-CONF-2004-005); Japan Atomic Energy Research Institute: Kashiwa, Japan, 2004.
23. Konno, C.; Ochiai, K.; Ohnishi, S. Insufficient self-shielding correction in VITAMIN-B6. *Prog. Nucl. Sci. Technol.* **2011**, *1*, 32–35. [CrossRef]
24. Pescarini, M.; Orsi, R.; Frisoni, M. Production and testing of the ENEA-Bologna VITJEFF32.BOLIB (JEFF-3.2) multi-group (199n+42γ) cross section library in AMPX format for nuclear fission applications. In *EPJ Web of Conferences*; EDP Sciences: Les Ulis, France, 2017; Volume 153, p. 07003.
25. Bondarenko, I.I. *Group Constants for Nuclear Reactor Calculations*; Consultants Bureau: New York, NY, USA, 1964.
26. Manturov, G.; Rozhikhin, Y.; Trykov, L. Neutron and Photon Leakage Spectra from Cf-252 Source at Centers of Six Iron Spheres of Different Diameters. In *ICSBEP Handbook, ALARM-CF-FE-SHIELD-001*; Organization for Economic Cooperation and Development-Nuclear Energy Agency (OECD-NEA): Paris, France, 2007.
27. Maekawa, F.; Yamamoto, J.; Ichihara, C.; Ueki, K.; Ikeda, Y. *Collection of Experimental Data for Fusion Neutronics Benchmark (No. JAERI-M-94-014)*; Japan Atomic Energy Research Institute: Tōkai, Japan, 1994.
28. Ghorai, S.K. *Determination of Neutron Flux Distribution by Using ANISN, a One-Dimensional Discrete S_N Ordinates Transport Code with Anisotropic Scattering*; NASA, Johnson (Lyndon B.) Space Center The 1983 NASA/ASEE Summer Faculty Fellowship Research Program Research Reports; NASA Johnson Space Center: Houston, TX, USA, 1983.
29. Forster, R.A.; Cox, L.J.; Barrett, R.F.; Booth, T.E.; Briesmeister, J.F.; Brown, F.B.; Bull, J.S.; Geisler, G.C.; Goorley, J.T.; Mosteller, R.D.; et al. MCNP™ version 5. *Nucl. Instrum. Methods Phys. Res. Sect. B Beam Interact. Mater. At.* **2004**, *213*, 82–86. [CrossRef]
30. Kabach, O.; Chetaine, A.; Darif, A.; Jalil, A.; Saidi, A.; Benchrif, A.; Amsil, H. Processing of the ENDF/B-VIII.0β6 neutron cross-section data library and testing with critical benchmarks, OKTAVIAN shielding benchmarks and the doppler reactivity defect benchmarks. *Ann. Univ. Craiova Phys.* **2018**, *28*, 78–98.

31. Trkov, A.; Griffin, P.J.; Simakov, S.P.; Greenwood, L.R.; Zolotarev, K.I.; Capote, R.; Aldama, D.L.; Chechev, V.; Destouches, C.; Kahler, A.C.; et al. IRDFF-II: A new neutron metrology library. *Nucl. Data Sheets* **2020**, *163*, 1–108. [[CrossRef](#)]
32. Hajji, A.; Coquelet-Pascal, C.; Blaise, P. Monte-Carlo interpretation of the JANUS Phase 1, Phase 2 and Phase 4 shielding experiments with TRIPOLI-4®. *Ann. Nucl. Energy* **2021**, *159*, 108333. [[CrossRef](#)]

Disclaimer/Publisher’s Note: The statements, opinions and data contained in all publications are solely those of the individual author(s) and contributor(s) and not of MDPI and/or the editor(s). MDPI and/or the editor(s) disclaim responsibility for any injury to people or property resulting from any ideas, methods, instructions or products referred to in the content.